

Picking the Right Specialist: Attentive Neural Process-based Selection of Task-Specialized Models as Tools for Agentic Healthcare Systems

Pramit Saha¹ Joshua Strong¹ Mohammad Alsharid² Divyanshu Mishra¹ J. Alison Noble¹

Abstract

Task-specialized models form the backbone of agentic healthcare systems, enabling the agents to answer clinical queries across tasks such as disease diagnosis, localization, and report generation. Yet, for a given task, a single “best” model rarely exists. In practice, each task is better served by multiple competing specialist models where different models excel on different data samples. As a result, for any given query, agents must reliably select the right specialist model from a heterogeneous pool of tool candidates. To this end, we introduce **ToolSelect**, which adaptively learns model selection for tools by minimizing a population risk over sampled specialist tool candidates using a consistent surrogate of the task-conditional selection loss. Concretely, we propose an Attentive Neural Process-based selector conditioned on the query and per-model behavioral summaries to choose among the specialist models. Motivated by the absence of any established testbed, we, for the first time, introduce an agentic Chest X-ray environment equipped with a diverse suite of task-specialized models (17 disease detection, 19 report generation, 6 visual grounding, and 13 VQA) and develop **ToolSelectBench**, a benchmark of 1448 queries. Our results demonstrate that ToolSelect consistently outperforms 10 SOTA methods across four different task families.

1. Introduction

Recent advances in large language models (LLMs) (Thirunavukarasu et al., 2023; Naveed et al., 2025) have enabled agentic systems (Naveed et al., 2025; Wang et al., 2024; Guo et al., 2024) that can plan, reason, and interact with external tools, raising the prospect of more capable

¹Department of Engineering Science, University of Oxford, United Kingdom ²Department of Computer Science, Khalifa University, Abu Dhabi, United Arab Emirates. Correspondence to: Pramit Saha <pramit.saha@eng.ox.ac.uk>.

Preprint. February 17, 2026.

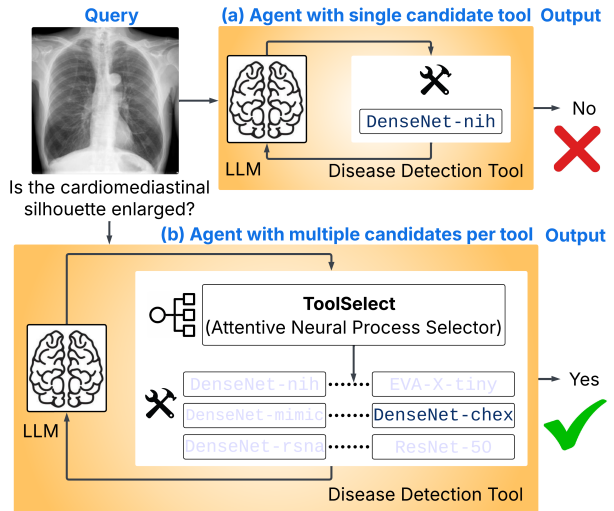


Figure 1. Why model selection for tools matters in agentic systems? **Top (a):** A naive setup with a single fixed specialist model per tool fails under domain and label-space mismatch. **Bottom (b):** Our approach equips tools with multiple specialist candidates and uses **ToolSelect** to adaptively select appropriate model for a given query, yielding more accurate clinical answers than (a).

AI assistants in healthcare (Qiu et al., 2024; Wang et al., 2025). However, in clinical settings, LLMs alone remain insufficient (Mofrad & Yousefzamani, 2025): they often lack up-to-date medical knowledge and expertise, struggle with domain-specific terminology and reasoning, and cannot directly solve complex clinical tasks based on high-dimensional data such as medical images and videos. As a result, agentic healthcare systems increasingly rely on task-specialized models as external tools to answer clinical queries precisely (Fallahpour et al., 2025a; Tang et al., 2025; Huang et al., 2026). These specialist models encapsulate domain expertise that general-purpose LLMs cannot reliably acquire through language-only training, making tool use a foundational component of practical clinical agents.

In real-world healthcare, a single tool per task is rarely sufficient. Clinical deployment faces substantial variability across hospitals, scanners, acquisition protocols, and patient populations, leading to pronounced domain shifts that can substantially degrade model reliability (Maleki et al., 2022;

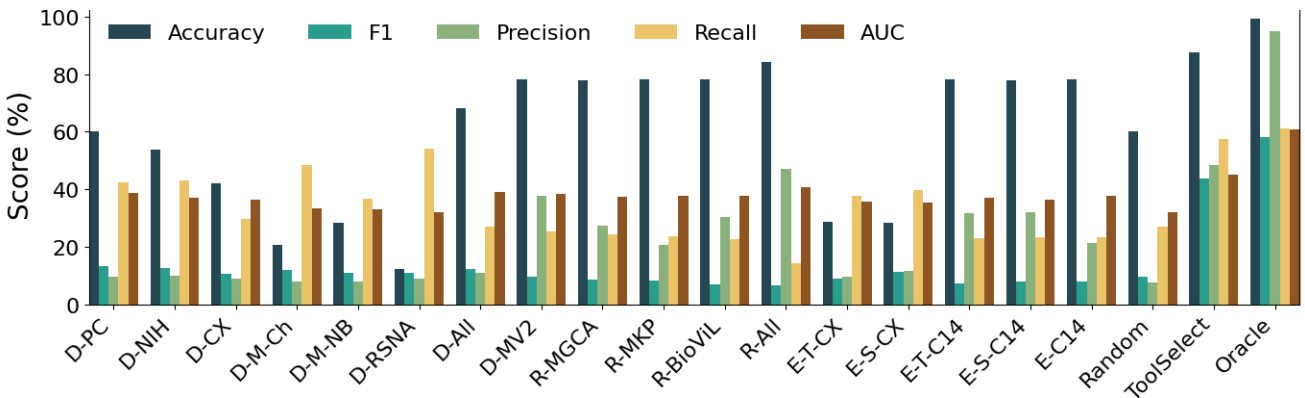


Figure 2. Performance comparison of **ToolSelect** against 18 task-specialized chest X-ray disease-detection models. Individual specialists exhibit low performance and substantial performance variability. The **Oracle** upper bound indicates that selecting the appropriate specialist per case can yield large gains, whereas **Random** selection often degrades performance, sometimes below that of individual models. **ToolSelect** consistently improves over individual specialists and random selection, aiming to close the gap to the Oracle.

Sanner et al., 2021; Musa et al., 2025). At the same time, training datasets differ in label definitions, granularity, and prevalence, creating label-space and label-distribution gaps that make “one-size-fits-all” training unrealistic. These issues are compounded by variable annotation quality, partial label coverage, heterogeneous reporting styles, and dataset-specific biases, as a result of which, models that perform well in one setting often fail to transfer to another. Therefore, practical agentic healthcare systems must maintain multiple task-specialized models as tools, covering different data regimes, label spaces, and clinical subpopulations. This makes tool candidate selection a pressing bottleneck in agentic healthcare systems. In other words, effective clinical performance depends not only on having access to a number of specialist candidate models as tools, but on reliably selecting the right one for each query.

In this paper, we study the problem of query-based tool candidate selection in agentic healthcare systems, *i.e.*, given a clinical query and a pool of specialized black-box models available for the selected task, we ask: *How can an agent reliably choose the most appropriate specialist for that specific input?* To address this, we introduce **ToolSelect**, a learning-based selection framework that performs query-based adaptive model selection within a task by minimizing a population risk over sampled candidate panels using a consistent surrogate of the task-conditional selection loss. ToolSelect represents each candidate model through compact behavioral summaries and employs an Attentive Neural Process selector conditioned on the query, enabling principled selection among heterogeneous specialists while keeping all underlying tools frozen (see Fig. 3).

To support rigorous evaluation in a realistic medical setting, we introduce an agentic chest X-ray environment with an LLM-based agent core and a diverse suite of task-specialized models spanning disease detection, report gen-

eration, visual grounding, and visual question answering (VQA). Subsequently, we develop a benchmark for investigating tool candidate selection called **ToolSelectBench** that instantiates the practical challenges motivating this work including domain shifts, mismatched label spaces, and partial label support within a single end-to-end agent workflow. This allows a systematic comparison of routing strategies under controlled but clinically meaningful tasks. Across ToolSelectBench, our proposed method consistently improves agent performance over a wide range of baselines. Our primary contributions can be summed up as follows:

- **Task, Framework, and Dataset contribution:** To the best of our knowledge, this is the first work to highlight (a) the importance of maintaining multiple specialist models as tool candidates in agentic healthcare systems and (b) the need for a query-conditioned tool-selection module that routes each request to an appropriate specialist. To enable reproducible study of this problem, we develop a testbed of 1448 Chest X-ray and question-answer triplets as well as a novel chest X-ray-based agentic environment comprising an inference-ready tool candidate pool spanning four task families: 17 disease-detection models, 19 report-generation models, 6 visual-grounding models, and 13 VQA models. These tools cover a broad range of diseases and clinical tasks and were either trained independently (from scratch or fine-tuned) or collected from diverse public sources. More details in §3.
- **Technical contribution:** We first formalize multi-task query-based tool candidate selection in agentic healthcare as a population-risk minimization problem over candidate models, each with partial task support. Building on this, we propose **ToolSelect**, a query-conditioned model selection method based on Attentive Neural Processes (ANP) and per-model behavioral summaries to select among available frozen specialist models. While we do not introduce new theorems, this work shows the importance of ANP-based

specialist model selection and comp-sum loss along with corresponding theoretical justification (See Suppl. B, C).

- **Empirical contribution:** We first investigate the standalone performance of 55 specialist models in our tool pool and release their outputs and responses to facilitate reuse and consistent evaluation without re-running training or inference. Additionally, we benchmark ToolSelect for each of the four Chest X-Ray-based task families against **12** diverse baselines spanning heuristic, ML-based selectors as well as LLM routing strategies adapted to tool selection setting.

2. Methodology

2.1. Problem formulation

Input and tasks. Each user query is a multimodal prompt $p = (x, q)$ consisting of an image $x \in \mathcal{X}$ and a natural-language instruction q (e.g., “Is there evidence of pneumonia in this chest X-ray?”). A task selector (LLM orchestrator) deterministically maps the prompt to a task $t = \tau(p) \in \mathcal{T}$ (e.g., disease detection, visual grounding, report generation, *etc.*).

Population of tools per task. For each task t , we assume a population distribution $P_t(E)$ over tool candidates (“specialists”). At inference time, the system observes an available panel: $S_t = (E_1, \dots, E_m) \sim P_t(E)^m$ with $m \geq 2$ (i.i.d. draws for simplicity). Each tool E_i provides a task-specific prediction rule g_E^t (e.g., class logits for disease detection) evaluated on inputs x . Tools may exhibit partial label-conditional support within a task, *i.e.*, for output components they cannot reliably predict, they emit a distinguished null prediction, implemented as a constant score in our experiments. Such tools still appear in S_t , but are automatically masked out for unsupported components during selection and loss computation to avoid interference.

Ground-truth outputs and costs. Let $y^t \in \mathcal{Y}_t$ denote the ground-truth output for task t (e.g., a disease label, correct MCQ option, an original report, or an expert-annotated bounding box). We evaluate each tool E_i using a bounded, task-specific cost $c_E^t(x, y^t) \in [0, 1]$ instantiated as follows:

- **Disease Detection:** $c_E^t(x, y) = \mathbb{1}[\arg \max g_E^t(x) \neq y]$, or calibrated cross-entropy clipped to $[0, 1]$.
- **Visual Grounding:** $c_E^t(x, y) = 1 - \text{IoU}(\hat{y}_E(x), y)$, where intersection over union (IoU) is evaluated between predicted and ground-truth regions for each instance.
- **Report Generation:** $c_E^t(x, y) = 1 - \text{F1}_{\text{RadGraph}}(\hat{y}_E(x), y)$, which measures structured clinical correctness between the generated report and ground truth per instance.
- **VQA:** $c_E^t(x, y) = \mathbb{1}[\hat{y}_E(x, q) \neq y]$ where $\hat{y}_E(x, q)$ is the option selected by VLM for the multiple-choice question q .

Partial support and abstention. Each tool may not provide meaningful predictions for all output components under a given task. We represent such abstentions via a distinguished null prediction and define a task-conditional validity indicator $\mathbb{1}[(x, t) \in \sigma_E]$, where σ_E denotes the support of tool E . The cost $c_E^t(x, y^t)$ is evaluated only on supported components. Tools outside the effective support are masked out for corresponding selection decision and contribute neither to loss nor to normalization of selection probabilities.

2.2. Tool candidate model selection

Selector. Given a prompt–task–panel tuple (p, t, S_t) , we define a parametric selector r_θ that assigns a real-valued score to each tool candidate in the available panel S_t . Formally,

$$r_\theta : (\mathcal{X} \times \mathcal{Q}) \times \mathcal{E}^m \rightarrow \mathbb{R}^m$$

$$(p, S_t) \mapsto (r_\theta(p, 1; S_t), \dots, r_\theta(p, m; S_t))$$

where $r_\theta(p, j; S_t)$ denotes the score assigned to the j -th tool E_j in the panel, conditioned on p and full panel context S_t . We convert these scores into selection probabilities $\pi_\theta(j | p, S_t)$ via a masked softmax:

$$\pi_\theta(j | p, S_t) = \frac{\exp(r_\theta(p, j; S_t)) \mathbb{1}[(x, t) \in \sigma_{E_j}]}{\sum_{k=1}^m \exp(r_\theta(p, k; S_t)) \mathbb{1}[(x, t) \in \sigma_{E_k}]}$$

where $\mathbb{1}[(x, t) \in \sigma_{E_j}]$ is a task-conditional validity indicator that masks out tools that do not support the current input–task pair. At inference time, the selected tool is

$$\hat{j}(p, S_t) = \arg \max_j \pi_\theta(j | p, S_t)$$

Task-conditional selection risk. For a single decision with panel S_t , the population selection loss is defined as:

$$L_{\text{sel}}^t(r_\theta; p, y^t, S_t) = \sum_{j=1}^m c_{E_j}^t(x, y^t) \mathbb{1}[\hat{j}(p, S_t) = j]$$

The population risk averages over data and panels:

$$E_{(X, Y^t) \sim D_t, S_t \sim P_t(E)^m} [L_{\text{sel}}^t(r_\theta; (X, q), Y^t, S_t)].$$

Comp-sum surrogate loss. Directly minimizing L_{sel} is intractable, as the induced selection rule is combinatorial and non-differentiable. We therefore adapt the comp-sum surrogate of the loss following (Mao et al., 2023b;a) to our tool candidate selection setting. For any decreasing function $\Psi : [0, 1] \rightarrow \mathbb{R}_+$ with $\Psi(1) = 0$, we define:

$$L_\Psi^t(r_\theta; p, y^t, S_t) = \sum_{j: E_j \text{ valid for } t} \left(\underbrace{\left(\sum_{j' \neq j} c_{E_{j'}}^t(x, y^t) - m + 2 \right)}_{w_j(p, y^t, S_t)} \right) \times \Psi(\pi_\theta(j | p, S_t))$$

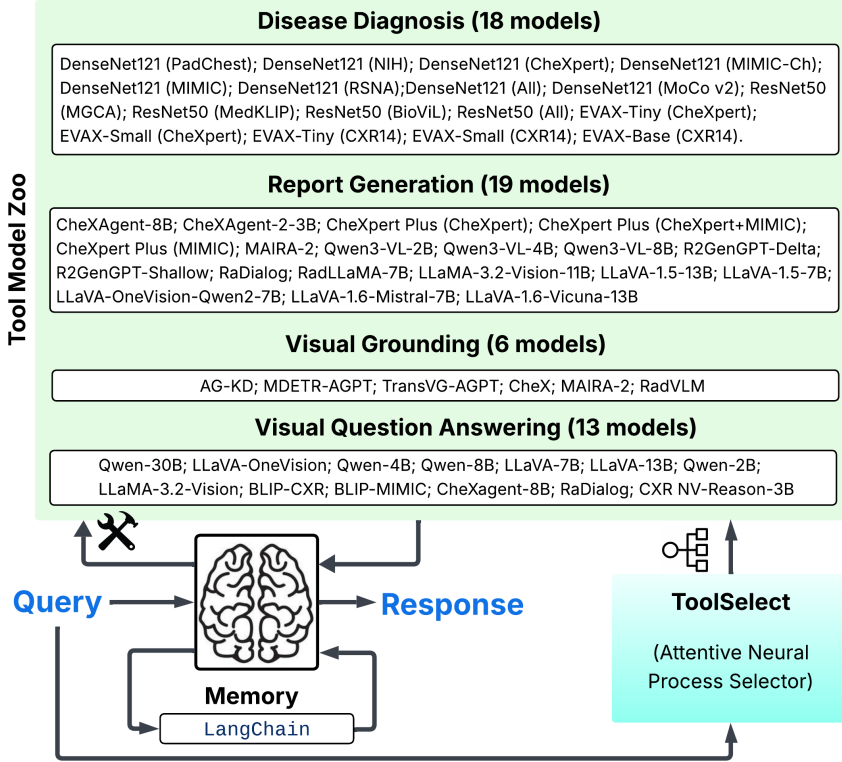


Figure 3. Architecture of our agentic framework. The system follows a ReAct-style loop, combining short-term memory (LangChain) with a heterogeneous tool model zoo incorporating fundamental Chest X-Ray-based tasks required to process user queries. Our proposed ToolSelect module is integrated to perform query-conditioned tool candidate (i.e., specialist model) selection.

Consequently, we train the selector by minimizing the task-marginalized objective (with λ_t as the task weights):

$$\mathcal{E}_\Psi(r_\theta) = \sum_{t \in \mathcal{T}} \lambda_t E_{(X, Y^t) \sim D_t, S_t} [L_\Psi^t(r_\theta; (X, q), Y^t, S_t)]$$

where λ_t are the task weights. In all experiments, we use the logistic comp-sum loss, $\Psi(u) = -\log u$. For $m = 2$, the surrogate reduces to a cost-sensitive binary margin form: $c_{E_2}^t \Phi(\Delta) - c_{E_1}^t \Phi(-\Delta)$ with $\Delta = r_\theta(p, 1) - r_\theta(p, 2)$.

2.3. Attentive Neural Process for tool candidate selection

Relation to meta-learning with reference sets. Our selector follows a model-based meta-learning paradigm for learning from tool-specific reference sets. In contrast to meta-optimization approaches which adapt parameters via gradient updates at test time, we condition the selector directly on a tool’s behavioural reference set through a single forward pass. We instantiate this conditioning using an Attentive Neural Process (ANP) (Kim et al., 2019), enabling query-dependent adaptation without test-time optimization.

Label-space alignment. Our tool candidates have heterogeneous output spaces \mathcal{Y}_E^t (e.g., different classes, phrase vocabularies or mask resolutions). We maintain a known mapping $\rho_E^t : \mathcal{Y}_E^t \rightarrow 2^{\mathcal{Y}_t}$ to a canonical task space

\mathcal{Y}_t . For classification, we compute aligned probabilities $\tilde{m}_E^t(x) \in \Delta^{|\mathcal{Y}_t| - 1}$ by summing over pre-image labels. When a tool does not support a particular label or component, $\tilde{m}_E^t(x)$ assigns a uniform (uninformative) score, which we treat as a null prediction and mask out during routing and loss computation.

Task-specific reference set (few-shot behavioural descriptors). To support query-guided selection, each specialist model E provides a small reference set:

$$D_E^t = \{d_{E,b}^t\}_{b=1}^{B_t}, \quad d_{E,b}^t = (x_b, y_b^t, m_E^t(x_b)),$$

which summarizes its behaviour on task t . Here $m_E^t(x_b)$ denotes the tool’s aligned prediction and B_t is kept intentionally small (tens of examples; $B_t \in [16, 64]$ in our experiments). In practice, B_t should be as large as possible while remaining feasible for tool maintenance (i.e., without incurring undue cost to produce or refresh predictions).

Query and tool encoders. We encode the input image, text, and instruction with task-shared backbones (ϕ_x, ϕ_q) :

$$\phi_x : \mathcal{X} \rightarrow \mathbb{R}^{d_x}, \quad \phi_q : \mathcal{Q} \rightarrow \mathbb{R}^{d_q},$$

$$u(p) = U[\phi_x(x) \parallel \phi_q(q)] \in \mathbb{R}^{d_u}.$$

Reference encoding. Each reference element is embedded:

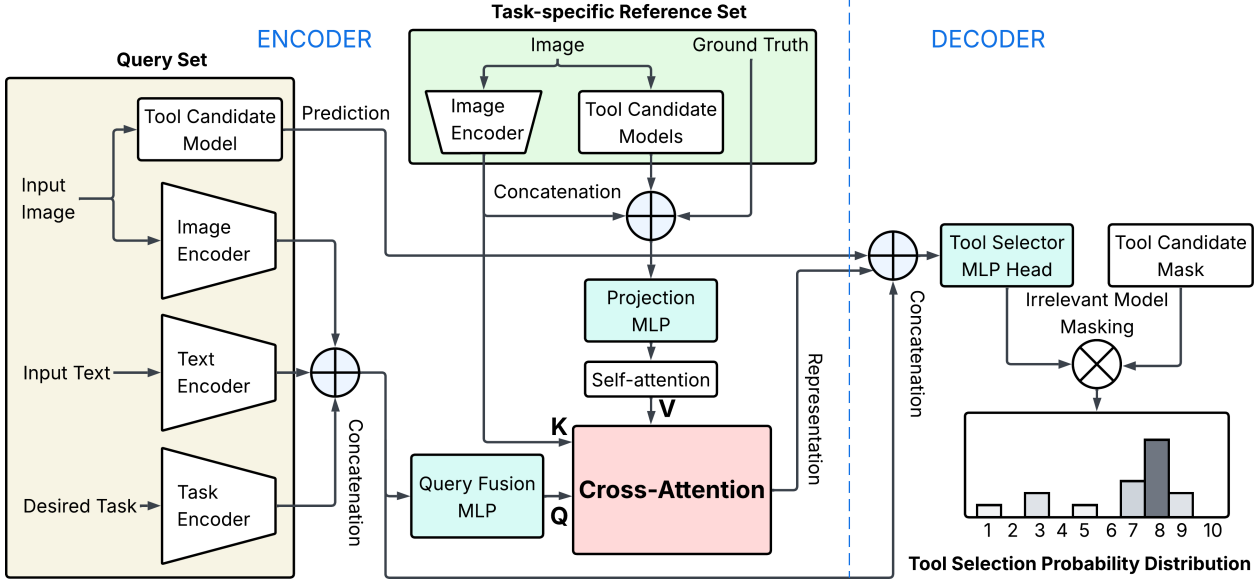


Figure 4. Overview of the proposed **ToolSelect** architecture. Given a multimodal query (image, text, and task), query features are fused and used to attend over task-specific per-tool reference sets that summarize each candidate tool’s empirical behavior. Cross-attention produces a query-conditioned representation for each tool, which is combined with the tool’s prediction and passed to a selector network. Tools that do not support the queried task are masked out before producing the final tool selection probability distribution.

$t_b = W_c [\phi_x(x_b) \parallel e^t(y_b^t) \parallel \rho_m(\tilde{m}_E^t(x_b))] \in \mathbb{R}^d, T = [t_1, \dots, t_{B_t}] \sim \text{Cat}(\lambda)$, a minibatch $\{(x_i, y_i^t, q_i)\}_{i=1}^B \sim D_t$, and, for each i , an available tool panel $S_t^{(i)} \sim P_t(E)^m$. We compute the scores $\{r_\theta(p_i, E; S_t^{(i)})\}$, form the selection probabilities π_θ , construct weights w_j from costs $c_{E_j}^t(x_i, y_i^t)$, and accumulate the comp-sum loss.

Reference self-attention and query–reference cross-attention. To obtain richer representations of the reference set, we next apply self-attention. Given query representation $u(p)$, we apply cross-attention between the query and the reference set:

$$\tilde{T} = \text{SelfAttn}(T), K = W_K [\phi_x(x_1), \dots, \phi_x(x_{B_t})]^\top, V = W_V \tilde{T}, z_E^t(p) = \text{softmax}\left(\frac{(W_Q u(p)) K^\top}{\sqrt{d_k}}\right) V \in \mathbb{R}^{d_v}.$$

The resulting vector $z_E^t(p)$ serves as a **query-dependent tool descriptor** $\psi_E^t(p)$, emphasizing those reference examples most relevant to the current input. This allows the selector to prefer tools that perform well on inputs similar to the query, even if they are not globally optimal on average.

Selector head. We score tool candidate model E as:

$$r_\theta(p, E; S_t) = g_\theta([u(p) \parallel \psi_E^t(p) \parallel \tilde{m}_E^t(x) \parallel \eta_E]),$$

with a lightweight MLP g_θ shared across tasks and η_E encodes optional tool metadata. The scores are normalized into $\pi_\theta(j \mid p, S_t)$ as described in §2.2.

2.4. Training objective and algorithm

Overall objective. We minimize $\mathcal{E}_\Psi(r_\theta)$ (see § 2.2) together with the regularizers described below. Gradients propagate through the router and the ANP encoders, while tool candidate models g_E^t are kept frozen. See Suppl. B & C.

Panel sampling. At each SGD step, we sample a task

Regularization. We employ two regularizers: (i) a *panel entropy* term $\lambda_H E[-\sum_j \pi_\theta(j) \log \pi_\theta(j)]$ to discourage over-confident selections early in training, and (ii) a per-tool *coverage head* $s_E^t(p) = \sigma(h([u(p) \parallel \psi_E^t(p)]))$, trained with targets $(1 - c_{E_j}^t)$ to approximate the tool’s task-conditional success probability.

3. Dataset and Experimental Setup

3.1. Tasks and Datasets

We consider four tool sets corresponding to fundamental tasks in chest X-ray-based clinical workflows: (i) disease diagnosis, (ii) report generation, (iii) phrase-level visual grounding, and (iv) multiple-choice VQA for chest X-Ray interpretation. For disease diagnosis, we construct evaluation queries using two external datasets, Open-I (Jaeger et al., 2014) and VinDr-CXR (Nguyen et al., 2022), which introduce clinically realistic domain shifts (e.g., scanner, acquisition protocol, and patient population) and label-distribution mismatch relative to the training sources of the candidate models. Similarly, for report generation, we use Open-I and for phrase-level grounding, we use VinDr-CXR. For multiple-choice VQA, we sample 1% of the ReX-VQA dataset (Pal et al., 2025). Across all tasks, we follow the

standard dataset splits: the training split is used for training the selector, and performance is reported on the corresponding test split. We construct **ToolSelectBench**, a unified benchmark comprising **550** disease diagnosis, **156** report generation, **394** phrase-level grounding, and **348** multiple-choice VQA queries, all drawn from the corresponding test set. All benchmark samples, together with the individual predictions of **55** candidate models, are attached as **supplementary material** for transparency and reproducibility.

3.2. Tool Candidate Model Zoo

Disease Diagnosis: We collected and/or trained 17 chest X-ray (CXR) models spanning three architectures: (a) DenseNet121, (b) ResNet50, and (c) ViT. The DenseNet121 models (Cohen et al., 2022) and their training data are: (i) DenseNet121–PadChest (D-PC), (ii) DenseNet121–NIH-CXR8 (D-NIH), (iii) DenseNet121–CheXpert (D-CX), (iv) DenseNet121–MIMIC-Ch (D-M-Ch), (v) DenseNet121–MIMIC-NB (D-M-NB), (vi) DenseNet121–RSNA-CXR (D-RSNA), (vii) DenseNet121–All-the-above-datasets (D-All), and (viii) DenseNet121–CXR-14, trained via MoCo-v2 (D-MV2). The ResNet50 models are: (i) ResNet50-CXR-14 trained via MGCA (R-MGCA), (ii) ResNet50-CXR14 trained via MedKLIP (RN50-MKP), (iii) ResNet50-CXR-14 trained via BioViL (R-BioViL), and (iv) ResNet50-All (R-All). Finally, our ViT-based models use the EVA-X foundation model (Yao et al., 2025) fine-tuned on respective datasets: (i) EVAX-Tiny–CheXpert (E-T-CX), (ii) EVAX-Small–CheXpert (E-S-CX), (iii) EVAX-Tiny–NIH-CXR14 (E-T-C14), (iv) EVAX-Small–NIH-CXR14 (E-S-C14), and (v) EVAX-Base–NIH-CXR14 (E-B-C14). Together, these models provide diversity across architecture families and sizes, training datasets, and training paradigms. The pool includes task-specialized models as well as models trained on large combined corpora and foundation-model variants, with different pretraining and supervision setups, to reflect realistic heterogeneity in clinical deployment.

Report Generation: We include 19 report-generation models spanning encoder–decoder, autoregressive, and multimodal LLM architectures. These comprise CheXAgent-8B, CheXAgent-2.3B, CheXpert Plus (CheXpert), CheXpert Plus (CheXpert+MIMIC), CheXpert Plus (MIMIC), MAIRA-2, Qwen3-VL-2B, Qwen3-VL-4B, Qwen3-VL-8B, R2GenGPT-Delta, R2GenGPT-Shallow, RaDialog, RadLLaMA-7B, LLaMA-3.2-Vision-11B, LLaVA-1.5-13B, LLaVA-1.5-7B, LLaVA-OneVision-Qwen2-7B, LLaVA-1.6-Mistral-7B, LLaVA-1.6-Vicuna-13B.

Visual Grounding: Our 6 grounding models span (i) dedicated phrase-grounding architectures (TransVG/MDETR) with medical pretraining (AGPT), (ii) knowledge-enhanced grounding (AG-KD), and (iii) multimodal radiology foundation models (ChEX, MAIRA-2, RadVLM), providing

complementary inductive biases and supervision styles.

Visual Question Answering: We include 13 diverse multimodal models spanning different model families and scales, including Qwen-based models (Qwen-2B/4B/8B/30B), LLaVA (7B, 13B, OneVision), LLaMA-3.2-Vision, BLIP models trained on CXR and MIMIC, as well as radiology-specific models such as CheXAgent-8B, RaDialog, and NVIDIA CXR NV-Reason-3B.

3.3. Training and Implementation details

We use a task-shared ViT-B/16 image encoder ϕ_x and CheXbert text encoder ϕ_q . The router head is a two-layer MLP (hidden width 512) with GELU activations. We optimize the logistic comp-sum surrogate using AdamW (learning rate 3×10^{-5} , weight decay 10^{-4}) for up to 50 epochs with early stopping (patience = 10, min_delta = 10^{-4}). The batch size is 16 for training, validation, and testing. Regularization includes panel entropy ($\lambda_H = 0.05$), an L_2 penalty on r_θ , and dropout of 0.1 in the ANP.

3.4. Baselines:

Due to absence of existing baselines for tool selection, we adapt 10 SOTA LLM-routers spanning instance-based, supervised, representation-learning, and structured routing paradigms. We include KNNRouter (Feng et al., 2025a) (nearest-neighbour retrieval over historical queries), SVM-Router (Feng et al., 2025b) and MLPRouter (supervised classifiers in embedding space), MFRouter (Ong et al., 2024) (matrix factorization learning latent query/model embeddings), EloRouter (Ong et al., 2024) (that selects the top-ranked model), RouterDC (Chen et al., 2024a) (dual-contrastive representation learning), AutoMix (Madaan et al., 2023) and Hybrid LLM (Ding et al.) (small-to-large model escalation based on confidence/quality-gap signals), GraphRouter (Feng et al.) (GNN-based routing over a query–model interaction graph), and CausallLM Router (Ong et al., 2024) (routing framed as generation, predicting the selected model name with a finetuned causal LLM).

4. Results and Analysis

4.1. Disease Diagnosis Performance

Table 1 shows that specialist models occupy markedly different points on the precision-recall trade-off, and these rankings shift substantially between Open-I and VinDr.

Failure modes and complementarity of specialist models: Table 1 shows that no single specialist is uniformly reliable under dataset shift, and conclusions depend strongly on the metric. For example, R-All attains the highest accuracy on both Open-I (84.08%) and VinDr (75.66%) but has the lowest F1 (Open-I 6.61%, VinDr 4.70%) and very low

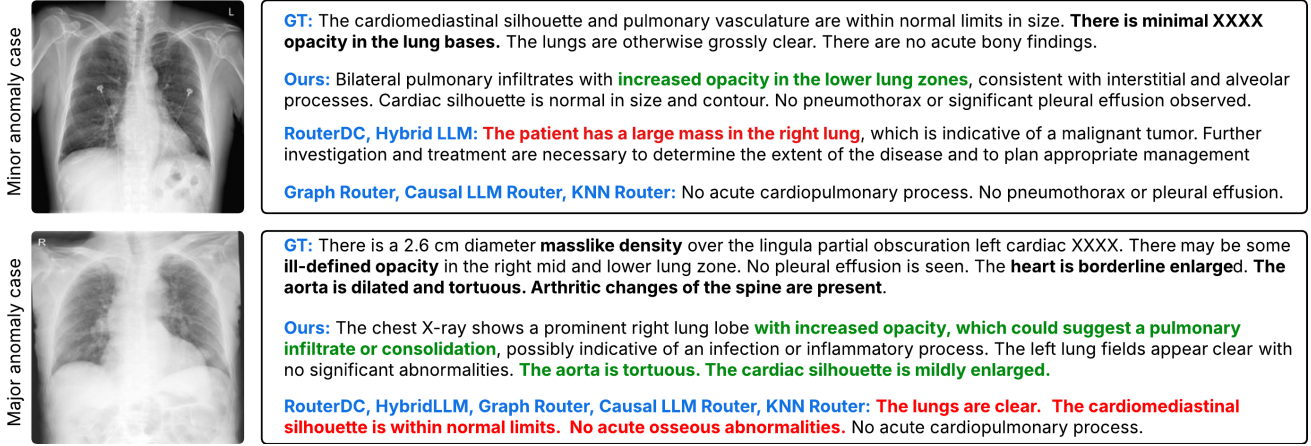


Figure 5. Qualitative report-generation comparison on minor (top) and major (bottom) anomaly cases (GT: ground truth). ToolSelect (ours) routes each query to the appropriate specialist, producing clinically aligned reports that emphasize the correct abnormal regions and severity. Baseline routers often hallucinate severity in minor cases or under-report major findings, yielding generic/misleading text; in the bottom case they all default to the globally strong CheXagent-8B and fail, whereas ToolSelect selects the better-suited CheXpert Plus model (despite lower average performance) and succeeds, highlighting the benefit of query-guided selection.

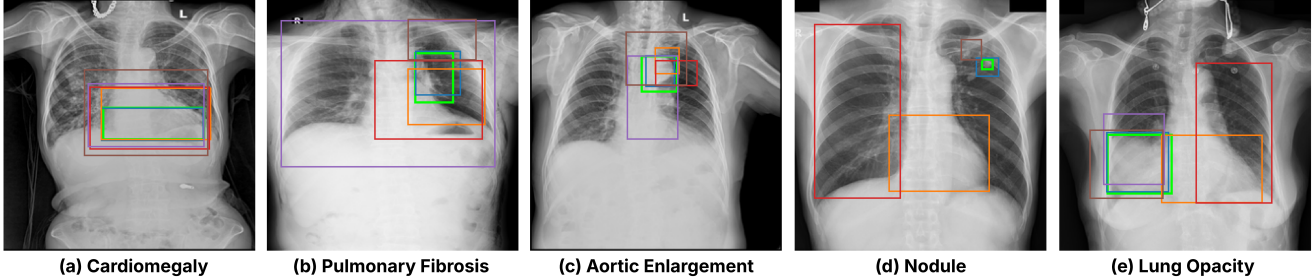


Figure 6. Qualitative phrase-level visual grounding results on chest X-rays. Green denotes the ground-truth box; blue denotes ToolSelect (ours); orange/red/brown/violet denote four baseline routers. ToolSelect consistently routes to a specialist that localizes the queried finding more tightly and accurately, while baselines often miss the target region or return overly coarse boxes that cover irrelevant area.

recall (Open-I 14.49%, VinDr 6.87%), reflecting a conservative regime that misses positives. In contrast, D-PC/D-NIH achieve higher Open-I recall (42.39%/42.93%) at low precision (~10%), indicating an over-calling regime, while MIMIC-trained models exhibit shift-induced miscalibration (e.g., D-M-Ch: recall 48.44% but Open-I accuracy 20.69%). The “best” model is context-dependent: candidates trade precision for recall differently across Open-I and VinDr (e.g., D-RSNA reaches 64.99% recall on VinDr but degrades sharply on Open-I). This matters clinically: high-recall specialists may be preferred for screening/ triage (e.g., D-RSNA 64.99%, D-M-Ch/D-M-NB 62.31%/62.27% recall on VinDr), whereas high-precision specialists may be preferred for prioritization/confirmation (e.g., R-BioViL 61.65%, E-S-C14 58.65% precision on VinDr).

Random vs. single specialists vs. oracle. Random routing is a lower bound when selection ignores query-specific information (Open-I: 9.54% F1/60.15% accuracy; VinDr: 20.81% F1/53.32% accuracy). The Oracle attains 58.00% F1 on Open-I and 66.22% on VinDr, indicating large head-

room from per-instance specialization. On VinDr, the best single-model F1 is only 24.81% (D-All/D-M-NB), close to Random, while Oracle is much higher, showing that the optimal specialist varies substantially across cases.

Baseline routers: Classical and heuristic routers give mixed improvements and can trail strong single tools. On Open-I, the best baseline F1 is MF Router at 11.98% (+2.44 over Random), while some achieve high accuracy but low F1 (e.g., RouterDC 81.52% accuracy vs 8.51% F1), consistent with conservative selection that misses positives. On VinDr, the best baseline F1 is Causal LLM at 24.44%, close to the best single-model F1 (24.81%) and far below Oracle (66.22%), indicating unreliable per-instance selection.

ToolSelect closes the Random–Oracle gap. ToolSelect consistently outperforms all baselines and captures a large fraction of the Oracle gap. On Open-I, it achieves 43.80% F1/87.64% accuracy, improving over the best baseline by +31.82 F1 points (vs 11.98%) and over the best single-model F1 by +30.45 (vs 13.35%). On VinDr, it achieves 59.88% F1/83.39% accuracy, improving over the best base-

Table 1. Comparison of disease-diagnosis performance (%) of individual tool candidates and tool selection methods. Acc: Accuracy; F1: F1 score; P: Precision; R: Recall. (all macro-averaged)

Method	Open-I					VinDr				
	Acc	F1	P	R	AUC	Acc	F1	P	R	AUC
Tool Candidate Models										
D-PC	60.22	13.35	9.72	42.39	38.74	49.32	22.12	20.06	46.86	41.16
D-NIH	53.88	12.54	9.85	42.93	36.91	35.50	23.90	17.86	51.70	37.21
D-CX	42.02	10.59	9.12	29.71	36.24	40.02	23.99	18.19	49.06	39.60
D-M-Ch	20.69	11.95	7.88	48.44	33.50	26.25	24.72	16.84	62.31	36.62
D-M-NB	28.21	10.82	7.91	36.71	33.16	26.04	24.81	16.89	62.27	37.43
D-RSNA	12.32	11.07	8.84	54.16	32.15	19.71	24.44	16.47	64.99	33.83
D-All	68.34	12.36	11.05	26.95	39.13	63.53	24.81	21.39	43.01	44.60
D-MV2	78.10	9.61	37.90	25.46	38.27	68.45	9.21	45.65	13.68	43.96
R-MGCA	77.96	8.61	27.39	24.29	37.46	68.68	10.69	44.37	14.56	46.71
R-MKP	78.17	8.21	20.73	23.83	37.73	68.77	10.83	51.60	14.51	45.61
R-BioViL	78.13	6.82	30.45	22.55	37.69	68.57	9.60	61.65	13.68	44.65
R-All	84.08	6.61	47.12	14.49	40.84	75.66	4.70	47.45	6.87	40.71
E-T-CX	28.63	9.12	9.54	37.83	35.67	34.21	20.82	21.48	47.24	39.74
E-S-CX	28.53	11.44	11.50	39.91	35.43	33.73	21.66	27.41	48.64	39.88
E-T-C14	78.21	7.37	31.84	22.90	37.19	68.72	10.21	53.87	14.32	47.98
E-S-C14	78.03	8.01	31.92	23.46	36.55	68.85	12.50	58.65	15.81	48.22
E-B-C14	78.13	7.97	21.20	23.35	37.76	68.91	13.06	48.91	16.09	48.24
Tool Selection Methods										
Random	60.15	9.54	7.56	27.19	32.20	53.32	20.81	18.19	32.07	39.01
AutoMix	51.14	10.53	16.07	23.56	35.68	51.67	20.96	18.28	33.32	37.06
SVM Router	33.33	11.76	13.70	37.59	36.77	72.58	13.18	27.37	14.01	41.32
Graph Router	12.32	11.07	8.84	54.16	32.15	68.71	10.24	53.24	14.34	46.00
MF Router	33.97	11.98	13.41	38.41	36.34	74.24	9.59	27.23	10.32	40.71
RouterDC	81.52	8.51	33.24	19.47	38.11	66.15	16.66	27.20	20.95	46.52
Hybrid LLM	66.13	8.00	13.80	19.06	35.58	67.21	18.27	27.09	20.32	46.66
KNN Router	30.16	11.52	11.63	38.75	35.09	74.23	8.92	26.04	9.83	41.18
Elo Router	28.53	11.44	11.50	39.91	35.43	75.66	4.70	47.45	6.87	40.71
MLP Router	33.69	9.01	11.46	31.92	34.29	73.33	12.24	29.12	12.59	40.83
Causal LLM	12.32	11.07	8.84	54.16	32.15	19.71	24.44	16.47	64.99	33.83
ToolSelect	87.64	43.80	48.55	57.31	45.09	83.39	59.88	68.62	65.15	49.91
Oracle	99.22	58.00	94.80	61.11	60.71	98.45	66.22	93.58	66.67	66.54

line by +35.44 F1 points (vs 24.44%) and over the best single-model F1 by +35.07 (vs 24.81%).

4.2. Report Generation

Consistent with diagnosis (§4.1), Table 2 shows large variability across report-generation tools and modest absolute performance. Radiology-tuned generators achieve the highest clinical correctness (CheXAgent-8B: 16.33% F1-RadGraph; CheXpert Plus (C+M): 16.10%), while several general-purpose VLMs degrade sharply (e.g., LLaVA-1.5-13B: 1.57%; LLaVA-1.5-7B: 3.05%), indicating that these models individually do not ensure clinical faithfulness.

Random vs. single vs. Oracle. Random selection yields limited correctness (F1-RadGraph 11.71%, RateScore 50.56). The best single generator reaches 16.33% F1-RadGraph (CheXAgent-8B), whereas Oracle attains 27.70% and 59.60 RateScore, revealing substantial per-instance heterogeneity and a large Oracle gap.

Baseline selectors. Baseline routers improve over Random, with MF Router at 22.40% F1-RadGraph and RouterDC at 16.01%, but remain well below Oracle (27.70%), suggesting limited ability to identify the best specialist per query.

ToolSelect. ToolSelect achieves the best routing performance (24.17% F1-RadGraph, 57.86 RateScore), improving over Random by +12.46 points and over the best single

Table 2. Report-generation performance across models (in %). C: CheXpert; M: MIMIC; C+M: CheXpert+MIMIC. R-L: ROUGE-L; MR: METEOR; F1-RG: F1-RadGraph; SemB: SemBScore; Rate: RateScore. Higher is better.

Model	Tool Candidate Models				
	SemB	F1-RG	R-L	MR	Rate
Tool Selection Methods					
CheXAgent-8B	41.91	16.33	21.97	25.00	55.06
CheXagent-2-3B	34.44	11.47	15.26	23.64	54.24
CheXpert Plus (C)	42.86	15.71	19.48	30.55	56.59
CheXpert Plus (C+M)	41.81	16.10	20.35	30.88	57.05
CheXpert Plus (M)	43.32	10.71	19.91	28.99	54.31
MAIRA-2	36.90	9.56	14.34	16.44	45.55
Qwen3-VL-2B	38.62	12.32	16.65	26.73	51.72
Qwen3-VL-4B	45.38	10.63	16.35	22.52	51.33
Qwen3-VL-8B	37.00	10.62	15.47	26.77	50.65
R2GenGPT-Delta	43.30	14.07	20.25	29.78	53.68
R2GenGPT-Shallow	40.41	15.56	20.37	30.73	52.95
RaDialog	35.28	11.04	20.13	25.22	50.31
RadLLaMA-7B	35.47	13.63	11.40	24.33	49.98
LLaMA-3.2-Vision-11B	26.71	7.00	13.49	20.15	47.26
LLaVA-1.5-13B	23.72	1.57	11.66	10.89	39.57
LLaVA-1.5-7B	20.37	3.05	12.10	12.28	40.09
LLaVA-OneVision-Qwen2-7B	25.84	9.37	15.32	22.19	48.78
LLaVA-1.6-Mistral-7B	26.84	8.53	13.08	19.97	46.85
LLaVA-1.6-Vicuna-13B	24.83	8.03	15.37	20.26	46.31
Tool Selection Methods					
Random	36.04	11.71	16.42	24.23	50.56
AutoMix	23.72	1.57	11.66	10.89	39.57
SVM Router	42.39	16.87	21.97	26.04	55.88
Graph Router	41.91	16.33	21.97	25.00	55.06
MF Router	46.53	22.40	21.77	31.25	56.76
RouterDC	41.89	16.01	20.27	30.61	56.94
Hybrid LLM	44.13	16.77	22.10	24.99	55.60
KNN Router	42.64	15.74	19.83	30.29	56.36
Elo Router	41.91	16.33	21.97	25.00	55.06
MLP Router	42.39	16.87	21.97	26.04	55.88
Causal LLM Router	42.59	15.74	19.54	30.39	56.83
ToolSelect (Ours)	47.92	24.17	22.44	32.51	57.86
Oracle	50.17	27.70	23.85	34.31	59.60

generator by +7.84, and surpassing the strongest baseline (MF Router) by +1.77 F1-RadGraph. Qualitative examples in Fig. 5 show that ToolSelect selects specialists that produce more clinically aligned reports than baseline routing. See Suppl. E.1 for **ablation on reference point / aggregation**.

4.3. Visual Grounding

Analysis of complementarity. Table 3 shows grounding is highly phrase-dependent: different specialists excel on different findings and no single candidate dominates. ChEX is the most consistently strong single tool (e.g., best on Atelectasis 49.44, Calcification 18.86, Cardiomegaly 71.50), suggesting it is effective for well-localized findings with consistent appearance and clear spatial supervision. However, clinically important crossovers remain: AG-KD is stronger on Aortic enlargement and Pulmonary fibrosis (22.55 vs 20.22), indicating better sensitivity to global morphology and diffuse chronic patterns, while RadVLM is best on ILD, suggesting stronger language–vision alignment for heterogeneous interstitial disease. Overall, the best tool depends on the image and phrase, not only on average performance. **Hard phrases and weak specialists.** Some phrases re-

Table 3. Per-phrase performance (in %) with grounding metrics appended (mAP and Mean IoU).

Model	Aortic enl.	Atel.	Calc.	Cardio.	Cons.	ILD	Infil.	Lung	Opac.	Nodule/Mass	Other les.	Pulm. fib.	mAP@0.25	mAP@0.5	Mean IoU
Tool Candidate Models															
AG-KD	66.25	33.41	17.33	70.12	39.45	22.90	31.48	28.71	7.58	12.70	22.55	45.84	32.96	40.66	
MDETR-AGPT	25.84	6.80	1.06	40.52	6.19	14.11	5.07	5.18	2.91	6.29	3.10	18.96	1.76	16.52	
TransVG-AGPT	14.37	5.98	1.74	41.52	13.12	13.24	11.57	5.92	2.23	4.08	1.73	16.83	3.22	14.06	
ChEX	53.00	49.44	18.86	71.50	54.31	14.21	35.99	32.65	13.71	27.72	20.22	59.69	39.42	40.25	
MAIRA-2	16.34	13.19	6.11	38.32	14.00	17.18	13.18	11.32	1.81	3.04	5.81	24.18	4.60	16.67	
RadVLM	18.99	29.90	10.24	52.96	25.02	23.78	19.71	16.92	5.52	11.32	14.29	39.51	18.45	23.14	
Tool Selection Methods															
Random	37.76	30.37	9.21	56.78	34.67	25.50	27.14	22.68	7.77	20.45	13.88	50.90	10.12	32.41	
AutoMix	65.73	40.25	5.59	69.05	45.80	29.61	39.71	31.54	8.01	19.97	18.57	54.13	35.21	45.94	
SVM Router	27.58	5.44	1.61	42.36	6.95	12.32	4.34	2.85	3.06	7.72	4.33	18.44	1.87	20.42	
Elo Router	27.61	5.44	1.61	42.36	6.95	12.32	4.34	2.85	3.06	7.72	4.33	18.44	1.87	20.43	
Graph Router	64.03	40.25	2.76	70.13	45.80	30.14	39.71	31.57	9.08	22.90	19.13	55.17	35.07	45.92	
MF Router	64.91	40.25	5.59	68.75	45.80	30.22	39.71	32.19	8.01	17.29	17.66	53.79	34.83	45.42	
RouterDC	51.16	39.55	3.11	65.13	30.71	28.69	37.50	21.30	8.05	5.89	15.20	46.25	27.12	38.79	
Hybrid LLM	59.88	39.70	2.78	50.17	33.97	31.79	37.11	28.34	5.27	16.10	14.75	45.49	30.20	38.38	
KNN Router	27.42	5.44	1.61	42.36	6.95	12.32	4.34	2.85	3.06	7.72	4.33	18.37	1.87	20.37	
Causal LLM Router	65.73	40.25	5.59	69.05	45.80	29.61	39.71	31.54	8.01	19.97	18.57	54.12	35.21	45.94	
MLP Router	27.58	5.44	1.61	42.19	6.95	12.32	4.34	2.85	3.06	7.72	4.33	18.44	1.87	20.38	
ToolSelect (Ours)	67.16	52.06	19.72	72.60	59.56	34.23	41.72	36.61	15.82	34.25	26.81	63.98	48.39	50.08	
Oracle	69.29	63.19	23.92	76.77	63.68	49.34	58.74	49.01	19.06	47.33	32.63	78.34	56.31	56.20	

Table 4. Comparison across VQA task (%). Top row: Tool candidates (Q30B:Qwen-30B; LOV:LLaVA-OneVision; Q4B:Qwen-4B; Q8B:Qwen-8B; L7B:LLaVA-7B; L13B:LLaVA-13B; Q2B:Qwen-2B; L3.2V:LLaMA-3.2-Vision; BCXR:BLIP-CXR; BMIM:BLIP-MIMIC; CXA:CheXagent-8B; RDlg:RaDialog; NV: NVIDIA CXR NV-Reason-3B). Bottom row: Selection methods.

Tool Candidates	Q30B	LOV	Q4B	Q8B	L7B	L13B	Q2B	L3.2V	BCXR	BMIM	CXA	RDlg	NV
VQA Acc (%)	60.63	58.91	57.76	56.32	54.60	53.74	53.16	33.05	25.00	23.60	47.41	38.51	63.22
Selection Methods	Random	KNN	SVM	MLP	MF	Elo	Graph	RouterDC	AutoMix	Hybrid LLM	Causal LLM	ToolSelect	Oracle
VQA Acc (%)	46.49	41.52	47.37	47.08	36.55	63.74	47.37	45.61	24.27	42.69	47.37	72.01	96.49

main challenging for all tools (e.g., Nodule/Mass peaks at only 13.71; “Other lesion” is modest across candidates), consistent with subtle lesions, IoU sensitivity to small mis-localizations, and annotation variability. We also observe weak specialists: MDETR-AGPT and TransVG-AGPT have low mean IoU (16.52 and 14.06) and near-zero performance on several phrases (e.g., Calcification, Nodule/Mass).

Random vs. specialists vs. Oracle and ToolSelect. Random routing is non-trivial (IoU 32.41) due to strong candidates (AG-KD/ChEX), but remains far from Oracle (56.20), and the gap to the best single model (40.66) indicates strong per-instance heterogeneity. As two specialists are already strong, many baseline selectors yield limited gains over choosing a strong fixed tool and weak routing can even hurt. ToolSelect nonetheless closes much of the Random–Oracle gap (mean IoU 50.08) and improves over the best individual grounding model by ≈ 10 IoU points, reaching mAP@0.5 48.39 (about +9 over the best single), demonstrating effective query-conditioned matching across phrases and images. See Fig. 6 for qualitative performance evaluation.

4.4. Visual Question Answering

Table 4 shows wide variation across VQA tools, with accuracy ranging from 23.60% (BLIP-MIMIC) to 63.22% (NV), and a tight cluster of Qwen and LLaVA variants around the 50% range. This suggests several candidates are similarly strong on average, motivating query-conditioned selection when the best tool varies by question.

Do tool selection methods help? ToolSelect improves beyond the best individual model, reaching 72.01% accuracy compared to the strongest single model at 63.22%. Random selection is poor (46.49%), far below the best individual tool and far below Oracle (96.49%). This very large Oracle gap indicates strong per-instance specialization. Importantly, many classical routers underperform strong single models (e.g., KNN 41.52%, Graph 47.37%), highlighting that learning to route is non-trivial and that weak routing can destroy the benefit of having strong specialists. The fact that ToolSelect closes a meaningful portion of this gap (to 72.01%) suggests it extracts predictive signals from the query and tool behavior to choose the correct specialist more often than naive or heuristic routing.

5. Conclusion

In this paper, we studied query-conditioned selection among heterogeneous task-specialized models as tools for agentic healthcare. To address this, we introduced **ToolSelect**, an Attentive Neural Process-based selector that conditions on the incoming query and per-tool behavioral summaries to route each request to an appropriate specialist model while keeping all tool models frozen. To enable systematic evaluation of tool candidate selection in a clinically grounded setting, we introduced an agentic chest X-ray environment with a diverse suite of specialist tools spanning disease diagnosis, report generation, vi-

sual grounding, and VQA, and developed **ToolSelectBench**. Across these task families, our results show substantial complementarity among individual specialist models and consistently demonstrate that our learned selection mechanism outperforms SOTA routing baselines. Overall, our findings indicate that reliable performance in multimodal clinical agentic pipelines depends not only on usage of single specialized tool but combination and selection of multiple models via query-conditioned tool selection mechanism.

Impact Statement

This paper studies tool selection in agentic machine learning systems, motivated by healthcare applications where multiple task-specialized models must be orchestrated reliably. Our primary goal is to advance the methodological foundations of model and tool selection by formalizing query-conditioned routing among heterogeneous candidates and demonstrating its effectiveness empirically. Potential positive impacts include improved reliability, efficiency, and transparency in agentic systems that integrate multiple pre-trained models, particularly in medical imaging and clinical decision-support workflows. By enabling agents to select appropriate specialist tools rather than invoking all available models, the proposed approach may reduce computational cost and support more structured, auditable system design. At the same time, our work does not propose autonomous clinical decision-making, and all medical use cases considered are intended to support, rather than replace, human expertise. As with any machine learning system applied in healthcare, improper deployment without clinical oversight could pose risks. These concerns are not unique to our method and reflect broader challenges in the safe integration of AI systems into medical practice. Overall, this work contributes to the development of agentic architectures in machine learning. We do not anticipate new ethical risks beyond those already well studied in the deployment of machine learning systems, particularly in healthcare, but emphasize that responsible use requires careful validation, transparency, and human-in-the-loop oversight.

References

Martian LLM router. <https://withmartian.com/>.

Notdiamond LLM router. <https://www.notdiamond.ai/>.

Unify LLM router. <https://unify.ai/>.

Aggarwal, P., Madaan, A., Anand, A., Potharaju, S. P., Mishra, S., Zhou, P., Gupta, A., Rajagopal, D., Kappaganthu, K., Yang, Y., et al. Automix: Automatically mixing language models. *arXiv preprint arXiv:2310.12963*, 2023.

Chen, L., Zaharia, M., and Zou, J. FrugalGPT: How to use large language models while reducing cost and improving performance. *arXiv preprint arXiv:2305.05176*, 2023a.

Chen, S., Jiang, W., Lin, B., Kwok, J., and Zhang, Y. Routerdc: Query-based router by dual contrastive learning for assembling large language models. *Advances in Neural Information Processing Systems*, 37:66305–66328, 2024a.

Chen, S., Wang, Y., Wu, Y.-F., Chen, Q.-G., Xu, Z., Luo, W., Zhang, K., and Zhang, L. Advancing tool-augmented large language models: Integrating insights from errors in inference trees. In *The Thirty-eighth Annual Conference on Neural Information Processing Systems*, 2024b. URL <https://openreview.net/forum?id=ZIpdu0cHYu>.

Chen, W., Ma, X., Wang, X., and Cohen, W. W. Program of thoughts prompting: Disentangling computation from reasoning for numerical reasoning tasks. *Transactions on Machine Learning Research*, 2023b. ISSN 2835-8856.

Chen, Z., Varma, M., Xu, J., Paschali, M., Veen, D. V., Johnston, A., Youssef, A., Blankemeier, L., Bluethgen, C., Altmayer, S., Valanarasu, J. M. J., Muneer, M. S. E., Reis, E. P., Cohen, J. P., Olsen, C., Abraham, T. M., Tsai, E. B., Beaulieu, C. F., Jitsev, J., Gatidis, S., Delbrouck, J.-B., Chaudhari, A. S., and Langlotz, C. P. A vision-language foundation model to enhance efficiency of chest x-ray interpretation, 2024c. URL <https://arxiv.org/abs/2401.12208>.

Chen, Z.-Y., Shen, S., Shen, G., Zhi, G., Chen, X., and Lin, Y. Towards tool use alignment of large language models. In *Proceedings of the 2024 Conference on Empirical Methods in Natural Language Processing*, pp. 1382–1400, 2024d.

Cohen, J. P., Viviano, J. D., Bertin, P., Morrison, P., Torabian, P., Guerrera, M., Lungren, M. P., Chaudhari, A., Brooks, R., Hashir, M., et al. Torchxrayvision: A library of chest x-ray datasets and models. In *International Conference on Medical Imaging with Deep Learning*, pp. 231–249. PMLR, 2022.

Ding, D., Mallick, A., Wang, C., Sim, R., Mukherjee, S., Rühle, V., Lakshmanan, L. V., and Awadallah, A. H. Hybrid llm: Cost-efficient and quality-aware query routing. In *The Twelfth International Conference on Learning Representations*.

Du, N., Huang, Y., Dai, A. M., Tong, S., Lepikhin, D., Xu, Y., Krikun, M., Zhou, Y., Yu, A. W., Firat, O., et al. Glam: Efficient scaling of language models with mixture-of-experts. In *International Conference on Machine Learning (ICML)*, 2022.

Fallahpour, A., Ma, J., Munim, A., Lyu, H., and Wang, B. Medrax: Medical reasoning agent for chest x-ray. *arXiv preprint arXiv:2502.02673*, 2025a.

Fallahpour, A., Ma, J., Munim, A., Lyu, H., and Wang, B. Medrax: Medical reasoning agent for chest x-ray, 2025b. URL <https://arxiv.org/abs/2502.02673>.

Fallahpour, A., Ma, J., Munim, A., Lyu, H., and Wang, B. Medrax: Medical reasoning agent for chest x-ray. *arXiv preprint arXiv:2502.02673*, 2025c.

Fedus, W., Zoph, B., and Shazeer, N. Switch transformers: Scaling to trillion parameter models with simple and efficient sparsity. *Journal of Machine Learning Research (JMLR)*, 2022.

Feng, T., Shen, Y., and You, J. Graphrouter: A graph-based router for llm selections. In *The Thirteenth International Conference on Learning Representations*.

Feng, T., Shen, Y., and You, J. Graphrouter: A graph-based router for LLM selections. *arXiv preprint arXiv:2410.03834*, 2024.

Feng, T., Zhang, H., Lei, Z., Han, P., Patwary, M., Shoeybi, M., Catanzaro, B., and You, J. Fusionfactory: Fusing llm capabilities with multi-llm log data. *arXiv preprint arXiv:2507.10540*, 2025a.

Feng, T., Zhang, H., Lei, Z., Yue, H., Lin, C., and You, J. Llmrouter: An open-source library for llm routing. <https://github.com/ulab-uiuc/LLMRouter>, 2025b. GitHub repository.

Gao, L., Madaan, A., Zhou, S., Alon, U., Liu, P., Yang, Y., Callan, J., and Neubig, G. Pal: Program-aided language models. In *International Conference on Machine Learning*, pp. 10764–10799. PMLR, 2023.

Gou, Z., Shao, Z., Gong, Y., yelong shen, Yang, Y., Huang, M., Duan, N., and Chen, W. ToRA: A tool-integrated reasoning agent for mathematical problem solving. In *The Twelfth International Conference on Learning Representations*, 2024.

Guo, T., Chen, X., Wang, Y., Chang, R., Pei, S., Chawla, N. V., Wiest, O., and Zhang, X. Large language model based multi-agents: A survey of progress and challenges. *arXiv preprint arXiv:2402.01680*, 2024.

Huang, J., He, R., Khan, D. Z., Mazomenos, E. B., Stoyanov, D., Marcus, H., Jiang, L., Clarkson, M. J., and Hoque, M. I. Surgical ai copilot: Energy-based fourier gradient low-rank adaptation for surgical llm agent reasoning and planning. 2026.

Jaeger, S., Candemir, S., Antani, S., Wang, Y.-X. J., Lu, P.-X., and Thoma, G. Two public chest x-ray datasets for computer-aided screening of pulmonary diseases. *Quantitative imaging in medicine and surgery*, 4(6):475, 2014.

Jiang, D., Ren, X., and Lin, B. Y. LLM-Blender: Ensembling large language models with pairwise ranking and generative fusion. In *Proceedings of the 61st Annual Meeting of the Association for Computational Linguistics (Volume 1: Long Papers)*, 2023.

Kim, H., Mnih, A., Schwarz, J., Garnelo, M., Eslami, A., Rosenbaum, D., Vinyals, O., and Teh, Y. W. Attentive neural processes. *arXiv preprint arXiv:1901.05761*, 2019.

Kim, Y., Park, C., Jeong, H., Chan, Y. S., Xu, X., McDuff, D., Lee, H., Ghassemi, M., Breazeal, C., and Park, H. W. Mdagents: An adaptive collaboration of llms for medical decision-making. In *The Thirty-eighth Annual Conference on Neural Information Processing Systems*, 2024.

Lee, C.-H., Cheng, H., and Ostendorf, M. OrchestraLLM: Efficient orchestration of language models for dialogue state tracking. In *Proceedings of the 2024 Conference of the North American Chapter of the Association for Computational Linguistics: Human Language Technologies (Volume 1: Long Papers)*, 2024.

Li, B., Yan, T., Pan, Y., Luo, J., Ji, R., Ding, J., Xu, Z., Liu, S., Dong, H., Lin, Z., et al. Mmedagent: Learning to use medical tools with multi-modal agent. In *Findings of the Association for Computational Linguistics: EMNLP 2024*, pp. 8745–8760, 2024.

Liu, W., Huang, X., Zeng, X., xinlong hao, Yu, S., Li, D., et al. ToolACE: Winning the points of LLM function calling. In *The Thirteenth International Conference on Learning Representations*, 2025. URL <https://openreview.net/forum?id=8EB8k6DdCU>.

Liu, Z., Hoang, T. Q., Zhang, J., Zhu, M., Lan, T., Kokane, S., Tan, J., Yao, W., Liu, Z., Feng, Y., N, R. R., Yang, L., Savarese, S., Niebles, J. C., Wang, H., Heinecke, S., and Xiong, C. APIGen: Automated Pipeline for generating verifiable and diverse function-calling datasets. In *The Thirty-eight Conference on Neural Information Processing Systems Datasets and Benchmarks Track*, 2024. URL <https://openreview.net/forum?id=Jfg3vw2bjx>.

Lu, P., Peng, B., Cheng, H., Galley, M., Chang, K.-W., Wu, Y. N., Zhu, S.-C., and Gao, J. Chameleon: Plug-and-play compositional reasoning with large language models. *Advances in Neural Information Processing Systems*, 36, 2024.

Madaan, A., Aggarwal, P., Anand, A., Potharaju, S. P., Mishra, S., Zhou, P., Gupta, A., Rajagopal, D., Kappagan-thu, K., Yang, Y., et al. Automix: Automatically mixing language models. *CoRR*, 2023.

Maleki, F., Ovens, K., Gupta, R., Reinhold, C., Spatz, A., and Forghani, R. Generalizability of machine learning models: quantitative evaluation of three methodological pitfalls. *Radiology: Artificial Intelligence*, 5(1):e220028, 2022.

Mao, A., Mohri, C., Mohri, M., and Zhong, Y. Two-stage learning to defer with multiple experts. *Advances in neural information processing systems*, 36:3578–3606, 2023a.

Mao, A., Mohri, M., and Zhong, Y. Cross-entropy loss functions: Theoretical analysis and applications. In *International conference on Machine learning*, pp. 23803–23828. pmlr, 2023b.

Mofrad, F. B. and Yousefzamani, M. Limitations of large language models in healthcare systems. In *Applications of Large Language Models (LLM) in Healthcare Systems*, pp. 234–262. Chapman and Hall/CRC, 2025.

Musa, A., Prasad, R., Onwualu, P., and Hernandez, M. A systematic review of cross-population shifts in medical imaging analysis with deep learning. 2025.

Narayanan Hari, S. and Thomson, M. Tryage: Real-time, intelligent routing of user prompts to large language models. *arXiv e-prints*, 2023.

Naveed, H., Khan, A. U., Qiu, S., Saqib, M., Anwar, S., Usman, M., Akhtar, N., Barnes, N., and Mian, A. A comprehensive overview of large language models. *ACM Transactions on Intelligent Systems and Technology*, 16(5):1–72, 2025.

Nguyen, H. Q., Lam, K., Le, L. T., Pham, H. H., Tran, D. Q., Nguyen, D. B., Le, D. D., Pham, C. M., Tong, H. T., Dinh, D. H., et al. Vindr-cxr: An open dataset of chest x-rays with radiologist’s annotations. *Scientific Data*, 9(1):429, 2022.

Ong, I., Almahairi, A., Wu, V., Chiang, W.-L., Wu, T., Gonzalez, J. E., Kadous, M. W., and Stoica, I. RouteLLM: Learning to route LLMs with preference data. *arXiv preprint arXiv:2406.18665*, 2024.

Pal, A., Lee, J.-O., Zhang, X., Sankarasubbu, M., Roh, S., Kim, W. J., Lee, M., and Rajpurkar, P. Rexvqa: A large-scale visual question answering benchmark for generalist chest x-ray understanding. *arXiv preprint arXiv:2506.04353*, 2025.

Parisi, A., Zhao, Y., and Fiedel, N. Talm: Tool augmented language models. *arXiv preprint arXiv:2205.12255*, 2022.

Patil, S. G., Zhang, T., Wang, X., and Gonzalez, J. E. Gorilla: Large language model connected with massive APIs. In *The Thirty-eighth Annual Conference on Neural Information Processing Systems*, 2024. URL <https://openreview.net/forum?id=tBRNC6YemY>.

Qin, Y., Liang, S., Ye, Y., Zhu, K., Yan, L., Lu, Y., Lin, Y., Cong, X., Tang, X., Qian, B., et al. Toolllm: Facilitating large language models to master 16000+ real-world apis. In *The Twelfth International Conference on Learning Representations*.

Qin, Y., Liang, S., Ye, Y., Zhu, K., Yan, L., Lu, Y., Lin, Y., Cong, X., Tang, X., Qian, B., et al. Toolllm: Facilitating large language models to master 16000+ real-world apis. *arXiv preprint arXiv:2307.16789*, 2023.

Qiu, J., Lam, K., Li, G., Acharya, A., Wong, T. Y., Darzi, A., Yuan, W., and Topol, E. J. Llm-based agentic systems in medicine and healthcare. *Nature Machine Intelligence*, 6(12):1418–1420, 2024.

Rafailov, R., Sharma, A., Mitchell, E., Manning, C. D., Ermon, S., and Finn, C. Direct preference optimization: Your language model is secretly a reward model. In *Thirty-seventh Conference on Neural Information Processing Systems*, 2023. URL <https://openreview.net/forum?id=HPuSIXJaa9>.

Rafailov, R., Sharma, A., Mitchell, E., Manning, C. D., Ermon, S., and Finn, C. Direct preference optimization: Your language model is secretly a reward model. *Advances in Neural Information Processing Systems*, 36, 2024.

Ren, X., Tang, J., Yin, D., Chawla, N., and Huang, C. A survey of large language models for graphs. In *Proceedings of the 30th ACM SIGKDD Conference on Knowledge Discovery and Data Mining*, pp. 6616–6626, 2024.

Riquelme, C., Puigcerver, J., Mustafa, B., Neumann, M., Je natton, R., Susano Pinto, A., Keysers, D., and Houlsby, N. Scaling vision with sparse mixture of experts. *Advances in Neural Information Processing Systems (NeurIPS)*, 2021.

Šakota, M., Peyrard, M., and West, R. Fly-swat or cannon? cost-effective language model choice via meta-modeling. In *Proceedings of the 17th ACM International Conference on Web Search and Data Mining*, 2024.

Sanner, A., Gonzalez, C., and Mukhopadhyay, A. How reliable are out-of-distribution generalization methods for

medical image segmentation? In *DAGM German Conference on Pattern Recognition*, pp. 604–617. Springer, 2021.

Schick, T., Dwivedi-Yu, J., Dessì, R., Raileanu, R., Lomeli, M., Hambro, E., Zettlemoyer, L., Cancedda, N., and Scialom, T. Toolformer: Language models can teach themselves to use tools. *Advances in Neural Information Processing Systems*, 36:68539–68551, 2023.

Sharma, N. Cxr-agent: Vision-language models for chest x-ray interpretation with uncertainty aware radiology reporting, 2024. URL <https://arxiv.org/abs/2407.08811>.

Shazeer, N., Mirhoseini, A., Maziarz, K., Davis, A., Le, Q., Hinton, G., and Dean, J. Outrageously large neural networks: The sparsely-gated mixture-of-experts layer. In *International Conference on Learning Representations*, 2016.

Shi, Z., Gao, S., Chen, X., Feng, Y., Yan, L., Shi, H., Yin, D., Ren, P., Verberne, S., and Ren, Z. Learning to use tools via cooperative and interactive agents. In *Findings of the Association for Computational Linguistics: EMNLP 2024*, pp. 10642–10657, 2024.

Shnitzer, T., Ou, A., Silva, M., Soule, K., Sun, Y., Solomon, J., Thompson, N., and Yurochkin, M. Large language model routing with benchmark datasets. *arXiv preprint arXiv:2309.15789*, 2023.

Srivatsa, K., Maurya, K. K., and Kochmar, E. Harnessing the power of multiple minds: Lessons learned from LLM routing. *arXiv preprint arXiv:2405.00467*, 2024.

Stripelis, D., Hu, Z., Zhang, J., Xu, Z., Shah, A., Jin, H., Yao, Y., Avestimehr, S., and He, C. Tensoropera router: A multi-model router for efficient LLM inference. *arXiv preprint arXiv:2408.12320*, 2024.

Tang, Q., Deng, Z., Lin, H., Han, X., Liang, Q., Cao, B., and Sun, L. Toolalpaca: Generalized tool learning for language models with 3000 simulated cases. *arXiv preprint arXiv:2306.05301*, 2023.

Tang, X., Zou, A., Zhang, Z., Li, Z., Zhao, Y., Zhang, X., Cohan, A., and Gerstein, M. Medagents: Large language models as collaborators for zero-shot medical reasoning. In *Findings of the Association for Computational Linguistics ACL 2024*, pp. 599–621, 2024.

Tang, Y., Wang, K., Chen, Y., and Zhou, G. Endoagent: A memory-guided reflective agent for intelligent endoscopic vision-to-decision reasoning. *arXiv preprint arXiv:2508.07292*, 2025.

Thirunavukarasu, A. J., Ting, D. S. J., Elangovan, K., Gutierrez, L., Tan, T. F., and Ting, D. S. W. Large language models in medicine. *Nature medicine*, 29(8):1930–1940, 2023.

Wang, L., Ma, C., Feng, X., Zhang, Z., Yang, H., Zhang, J., Chen, Z., Tang, J., Chen, X., Lin, Y., et al. A survey on large language model based autonomous agents. *Frontiers of Computer Science*, 18(6):186345, 2024.

Wang, W., Ma, Z., Wang, Z., Wu, C., Ji, J., Chen, W., Li, X., and Yuan, Y. A survey of llm-based agents in medicine: How far are we from baymax? *arXiv preprint arXiv:2502.11211*, 2025.

Wu, Q., Bansal, G., Zhang, J., Wu, Y., Li, J., et al. Autogen: Enabling next-gen llm applications via multi-agent conversation. In *ICLR 2024 Workshop on Large Language Model (LLM) Agents*.

Wu, Q., Liu, W., Luan, J., and Wang, B. Toolplanner: A tool augmented llm for multi granularity instructions with path planning and feedback. In *Proceedings of the 2024 Conference on Empirical Methods in Natural Language Processing*, pp. 18315–18339, 2024.

Yao, J., Wang, X., Song, Y., Zhao, H., Ma, J., Chen, Y., Liu, W., and Wang, B. Eva-x: A foundation model for general chest x-ray analysis with self-supervised learning. *npj Digital Medicine*, 8(1):678, 2025.

Yao, S., Zhao, J., Yu, D., Du, N., Shafran, I., Narasimhan, K. R., and Cao, Y. React: Synergizing reasoning and acting in language models. In *The Eleventh International Conference on Learning Representations*.

Yuan, S., Song, K., Chen, J., Tan, X., Shen, Y., Ren, K., Li, D., and Yang, D. Easytool: Enhancing llm-based agents with concise tool instruction. In *ICLR 2024 Workshop on Large Language Model (LLM) Agents*.

Yue, M., Zhao, J., Zhang, M., Du, L., and Yao, Z. Large language model cascades with mixture of thought representations for cost-efficient reasoning. In *International Conference on Learning Representations (ICLR)*, 2024a.

Yue, X., Qu, X., Zhang, G., Fu, Y., Huang, W., Sun, H., Su, Y., and Chen, W. MAmmoTH: Building math generalist models through hybrid instruction tuning. In *The Twelfth International Conference on Learning Representations*, 2024b.

Zhao, W. X., Zhou, K., Li, J., Tang, T., Wang, X., Hou, Y., Min, Y., Zhang, B., Zhang, J., Dong, Z., et al. A survey of large language models. *arXiv preprint arXiv:2303.18223*, 2023.

Zhuang, Y., Chen, X., Yu, T., Mitra, S., Bursztyn, V., Rossi, R. A., Sarkhel, S., and Zhang, C. Toolchain*: Efficient action space navigation in large language models with a* search. In *The Twelfth International Conference on Learning Representations*.

Zuo, K., Jiang, Y., Mo, F., and Lio, P. Kg4diagnosis: A hierarchical multi-agent llm framework with knowledge graph enhancement for medical diagnosis. *arXiv preprint arXiv:2412.16833*, 2024.

A. Related Work

Healthcare Agents. Current medical agentic systems largely follow two complementary directions: (i) collaborative reasoning setups that aggregate multiple LLM/VLM outputs via debate or voting to improve reliability (Kim et al., 2024; Tang et al., 2024; Zuo et al., 2024), and (ii) tool-using agents in which an orchestrator coordinates task-specialized medical models (Li et al., 2024; Fallahpour et al., 2025c). Alongside these developments, medical VLMs are increasingly being packaged into agentic pipelines for chest X-ray understanding, extending beyond perception to structured reasoning, diagnostic prediction, and report generation. For example, MedRAX (Fallahpour et al., 2025b) integrates multiple perception modules with multimodal LLM reasoning to answer complex queries spanning VQA and reporting, while CXR-Agent (Sharma, 2024) produces structured reports together with diagnostic outputs, and CheXAgent (Chen et al., 2024c) aims for unified chest X-ray understanding across reasoning-oriented tasks. More broadly, MDAGents (Kim et al., 2024) adaptively configures multi-agent collaboration based on task complexity and reports strong benchmark performance, whereas MMedAgent (Li et al., 2024) selects and composes imaging tools (e.g., segmentation, classification, report generation) across five modalities. However, as medical agents become more prevalent and increasingly tool-dependent, most work emphasizes tool *orchestration* at a workflow level, while the problem of *query-conditioned selection* among multiple competing tool candidates for a given subtask remains largely unexplored. This motivates our focus on tool candidate selection in this paper.

Tool Augmented LLMs. Tool augmented LLM has emerged as a central mechanism for extending LLM problem-solving capabilities by enabling interaction with external tools, thereby alleviating limitations such as stale knowledge and lack of real-time data access (Zhao et al., 2023; Ren et al., 2024). Early work on tool-augmented language models (TALM) (Parisi et al., 2022) demonstrated that self-play can improve reasoning and mathematical performance, while Toolformer (Schick et al., 2023) showed that LLMs can self-supervise the acquisition of API-usage skills by integrating tool calls directly into text generation. As interest in tool use grew, subsequent efforts increasingly focused on constructing benchmarks and datasets to train and evaluate tool-using models, including agent-driven data generation (Tang et al., 2023), bootstrapping from curated seed examples (Patil et al., 2024), adapting existing datasets, and scaling supervision with strong LLMs such as GPT-4 (Qin et al., 2023).

Broadly, prior work on tool learning follows two complementary directions. The first relies on prompt-based orchestration with powerful closed-source LLMs (Shi et al., 2024; Wu et al.; Yuan et al.; Chen et al., 2023b; Gao et al., 2023), evolving from ReAct’s (Yao et al.) thought-action prompting toward more structured multi-tool reasoning frameworks. Representative examples include Chameleon (Lu et al., 2024), which improves compositional reasoning by coordinating multiple tools with GPT-4, and ToolChain (Zhuang et al.), which enhances efficiency by searching the action space using A*. The second direction focuses on improving open-source LLMs through instruction tuning for tool use (Gou et al., 2024; Yue et al., 2024b; Chen et al., 2024d; Wu et al., 2024; Shi et al., 2024). ToolBench (Qin et al.) marked a major step in this line by curating a large-scale dataset covering 16,464 real-world APIs and introducing ToolLLM with depth-first decision-tree trajectory annotation, albeit with later work identifying limitations due to dataset quality. Building on this foundation, TP-LLaMA (Chen et al., 2024b) incorporates preference learning to leverage failed tool-use trajectories via DPO (Rafailov et al., 2023; 2024). More recent automated data-generation frameworks, such as APIGen (Liu et al., 2024) and Tool-Ace (Liu et al., 2025), further strengthen tool-use capabilities through multi-stage API validation and diversified query generation.

Despite this rapid progress, much of the existing literature focuses on learning to invoke individual APIs or execute short tool-use sequences. In contrast, we study tool use in medical agentic systems where tools correspond to task-specific clinical solvers (e.g., diagnosis, grounding, report generation, etc) with heterogeneous and partially overlapping capabilities; while prior work largely emphasizes learning to invoke tools or execute tool chains, it does not address query-conditioned selection among multiple competing specialist tool candidates in clinically realistic settings, which is the central focus of this paper.

LLM Routing. LLM routing has emerged as a central mechanism for controlling accuracy–cost trade-offs in systems that serve multiple large language models. Broadly, LLM routers act as control planes that decide which underlying model(s) should handle a given query, typically without modifying the query or the model outputs themselves. A prominent class of such systems performs prescriptive routing, where a lightweight learned classifier estimates query complexity or expected utility and routes the query to one of two (or more) candidate LLMs accordingly (Ding et al.; Ong et al., 2024; Stripelis et al., 2024; Šakota et al., 2024; Lee et al., 2024). In this setting, routing thresholds can be calibrated on representative workloads to achieve a desired balance between response quality and inference cost. An alternative paradigm is non-prescriptive routing, where routing decisions depend on the responses generated by candidate models rather than solely on the input query (Chen et al., 2023a; Aggarwal et al., 2023; Yue et al., 2024a). For example, FrugalGPT (Chen et al., 2023a) employs a

cascade of models ordered by cost, sequentially invoking models until a response satisfies a learned sufficiency criterion. Such approaches trade increased latency for improved cost efficiency by avoiding unnecessary invocation of stronger models.

Beyond cost-centric motivations, several routing methods focus primarily on improving response quality by exploiting complementary strengths of different models (Shnitzer et al., 2023; Narayanan Hari & Thomson, 2023; Feng et al., 2024; Srivatsa et al., 2024). These methods often frame routing as a learned matching problem between queries and model capabilities, using representations of queries, models, or their interactions to guide selection. Related but distinct are ensemble-style control mechanisms, such as mixture-of-experts (MoE) architectures (Du et al., 2022; Fedus et al., 2022; Riquelme et al., 2021; Shazeer et al., 2016), which dynamically select subsets of experts at the token level and combine their outputs. LLM synthesis approaches (Jiang et al., 2023) operate at the query level, routing entire inputs to multiple models and aggregating their responses. While these architectures can reduce inference costs and improve robustness, they differ fundamentally from routing systems in that they actively combine model outputs rather than selecting a single model per query. A primary application of LLM routing is cost reduction in LLM-powered services. Several commercial platforms, including Unify (uni), Martian (mar), and NotDiamond (not), offer routing-as-a-service solutions that transparently select an appropriate model for each query. By inserting a routing layer between applications and LLM providers, these systems report substantial cost savings - up to orders of magnitude in some deployments, while maintaining acceptable performance. Together, these developments underscore the growing importance of routing and orchestration mechanisms as foundational infrastructure for scalable LLM-based systems. Despite extensive work on LLM routing for cost and quality optimization, existing approaches largely focus on selecting among homogeneous language models and do not address the problem of query-conditioned selection among heterogeneous, task-specialized tools with partial and overlapping support. This gap motivates our focus on tool selection rather than LLM routing in this paper.